Granular segregation in the double-cone blender: Transitions and mechanisms

Albert W. Alexander, Troy Shinbrot, and Fernando J. Muzzio

Citation: Physics of Fluids **13**, 578 (2001); doi: 10.1063/1.1347961
View online: http://dx.doi.org/10.1063/1.1347961
View Table of Contents: http://scitation.aip.org/content/aip/journal/pof2/13/3?ver=pdfcov
Published by the AIP Publishing

Articles you may be interested in

Experimental investigation into segregating granular flows down chutes
Phys. Fluids **23**, 013301 (2011); 10.1063/1.3536658

Size Segregation in Dry Granular Flows of Binary Mixtures
AIP Conf. Proc. **1227**, 363 (2010); 10.1063/1.3435406

Dense Granular Flows: Rheology and Segregation
AIP Conf. Proc. **1027**, 938 (2008); 10.1063/1.2964900

Segregation induced instabilities of granular fronts
Chaos **9**, 621 (1999); 10.1063/1.166435

Axial segregation of granular materials
Chaos **9**, 573 (1999); 10.1063/1.166431

Did your publisher get
18 MILLION DOWNLOADS in 2014?
AIP Publishing did.

AIP Publishing THERE'S POWER IN NUMBERS. Reach the world with AIP Publishing.

This article is copyrighted as indicated in the article. Reuse of AIP content is subject to the terms at: http://scitation.aip.org/termsconditions. Downloaded to IP: 132.203.227.63 On: Sun, 12 Jul 2015 01:44:53

Granular segregation in the double-cone blender: Transitions and mechanisms

Albert W. Alexander, Troy Shinbrot, and Fernando J. Muzzio[a)]
Department of Chemical and Biochemical Engineering, Rutgers University, Piscataway, New Jersey 08854

(Received 23 February 2000; accepted 10 November 2000)

We investigate granular segregation in one of the most common industrial devices used in granular processing: the double-cone blender. We report several new and spontaneously occurring segregation patterns, including stripes, bands, and a symmetry-breaking state in which one species vacates half the tumbler. By varying the tumbling speed along with particle size and size ratio, we find that the transitions between segregated patterns are extremely sharp: Changes in fill level or speed of under one percent are sufficient to produce a reproducible qualitative change in the observed pattern. We show that the several distinct segregation patterns observed experimentally can be reproduced from a simplified model in which outward rolling on the convective granular cascade competes against inertial motion of rapidly moving large particles. Finally, we identify a cutoff particle size ratio above which large particles become buried in the cascading flow, and segregation appears to cease. © *2001 American Institute of Physics.* [DOI: 10.1063/1.1347961]

I. INTRODUCTION

Processing of mixtures of dissimilar grains almost invariably promotes segregation, characterized by the emergence of regions of differing composition. Many particle properties play a role in segregation, including size, density, shape, and cohesivity. Size segregation has drawn the greatest attention in the literature, including studies of fluidized beds,[1] tumbling blenders,[2] chutes,[3] hoppers,[4] and vibrated beds.[5] In this study, we examine segregation transitions in a common tumbling blender geometry: the double-cone [Fig. 1(a)]. Despite its widespread use, the double-cone has received little attention in the literature. Chester *et al.*, Brone and Muzzio, Carley-Macauley and Donald, and Sethuraman and Davies studied the effects of process parameters such as RPM and baffle addition on mixing efficiency of nonsegregating mixtures.[6] Additionally, Ashton and Valentin, Gray, and Kaufman used double-cones as a standard for comparison with other blenders; in these studies, all the blenders tested gave similar results.[7] Also, Ramanujan studied a segregating mixture, however, pattern formation was not reported nor was the effect of size ratio investigated.[8] Finally, Moakher *et al.* used experiments and particle-dynamic simulations to analyze robust segregational tendencies that persist in the double-cone as well as other 3D blender geometries.[9]

Other than these studies, the next closest system examined is the simple rotating drum, which has been the subject of much more extensive research. Recently, several groups of researchers focused on the formation and dynamic behavior of bands that form when a binary mixture is tumbled in a drum blender.[10] Most germane to the present work are the following.

Hill and Kakalios[11] defined three separate states: reversible segregation, irreversible segregation, and no segregation. These authors characterized the effect of particle size ratio, Φ, on the segregation state in a drum blender of aspect ratio ~ 5, and found that the state changed with Φ nonmonotonically, noting that small changes in system parameters can have large effects on segregating behavior.

In a similar vein, Bytnar *et al.*[12] studied segregation in a drum, in this case with aspect ratio 1, and identified five separate types of behavior: core segregation, transition, mixing, reverse segregation, and centrifuging. Bytnar *et al.* found that segregation occurs at very low and very high speeds for $\Phi < 3.1$, and that transitions between coring and mixing behaviors are found near Froude number[13] $\mathrm{Fr} \approx 0.25$, while near $\mathrm{Fr} \approx 0.75$ centrifuging takes over. Below $\Phi \approx 1.3$, a marked increase was found in the Froude number at which the transitions between these states occur; this increase was attributed to an inability of small particles to slip through gaps between larger particles. In similar work on V-blenders and drum tumblers, Carstensen and Patel[14] found that segregation decreases when Φ exceeds 2.5.

Williams and Khan,[15] on the other hand, studied the effects of particle diameter ratio and absolute particle size on segregation in an inclined drum mixer. Here it was found that a measure of segregation increases with Φ up to $\Phi \approx 4.3$ and then remains constant; moreover, it was determined that keeping Φ constant and lowering the mean particle diameter reduces the effects of segregation. These results were obtained using blends of fertilizer and sand; it was noted that glass particles show a decrease in segregation for $\Phi > 2.4$ which was attributed to triboelectrification. Thus in both the inclined drum and the V-blender, segregation appears to peak near $\Phi \approx 2.4$—although different authors attribute this to different causes, and although the precise point at which this peak occurs is different in each study and may be affected by particle characteristics and system scaling.

To summarize, at the present time, mechanisms for seg-

a)Author to whom correspondence should be addressed; electronic mail: muzzio@sol.rutgers.edu

 © 2001 American Institute of Physics
This article is copyrighted as indicated in the article. Reuse of AIP content is subject to the terms at: http://scitation.aip.org/termsconditions. Downloaded to IP: 132.203.227.63 On: Sun, 12 Jul 2015 01:44:53

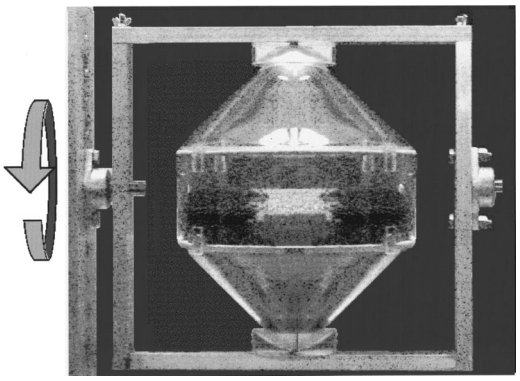

FIG. 1. Segregation state in double-cone. Transparent laboratory double-cone blender, showing typical segregation pattern between 4 mm (dark) and 1.6 mm (light gray) particles after tumbling through 200 revolutions at 25 rpm. Color versions of this and other figures are available at http://sol.rutgers.edu/~shinbrot/public_html/OnlinePapers/DConeSeg.pdf

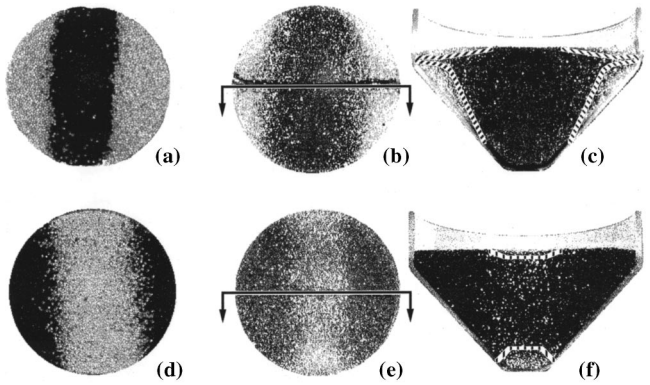

FIG. 2. Top and interior views of segregation patterns in 4.3 l and 0.5 l double-cone blenders. (a)–(c) show ''big-out'' pattern in 4.3 l (a) and 0.5 l (b)–(c) blenders; (d)–(f) show ''small-out'' pattern in the same blenders. In all cases, the tumblers were charged with 70% small (1.6 mm for large blender or 0.6 mm for small blender) and 30% large (4 mm for large blender or 1.6 mm for small blender) particles by volume, with the small particles loaded beneath the large. The large tumbler was filled to 50% of total volume; the small to 40%. The rotation speeds for these experiments were: (a) 23.1 rpm; (b)–(c) 27.6 rpm; (d) 28.4 rpm; (e)–(f) 32.9 rpm. (b) and (e) show the slicing plane (arrows) corresponding to views (c) and (f). (c) and (f) show interior views, with approximate boundaries between large and small grains identified by broken lines.

regation even in the simple tumbling drum remain unclear, and work on more complex, but industrially common, blender geometries is extremely limited. In the present work, we identify several previously unreported segregation states in the double-cone blender and examine mechanisms accounting for their formation. In Sec. II we describe the phenomenology seen in the double-cone, and in Sec. III we identify transitions between distinct segregated states. Finally, in Sec. IV we assess mechanisms believed to be responsible for these behaviors and investigate particle size effects that appear to cause segregation to vanish.

II. APPARATUS AND MATERIALS

The experiment is summarized here; details appear in Ref. 16. The tumbling vessels are custom-made acrylic containers consisting of two cones attached to a cylindrical midsection [Fig. 1(a)]. The vessel is held in a housing that is rotated by a stepper motor. Double-cone blenders are generally tumbled at a constant speed; in each of our experiments the rotation rate is fixed at a value in the range 8–40 rpm.[17] The effects of varying the size ratios of binary glass bead mixtures were examined using 4.3 l and 0.5 l double-cone blenders i.e., smaller-scale experiments are run in a double-cone with linear dimensions that are approximately half those of the large double-cone. In some experiments, the contents of this vessel are ''frozen'' in place by infiltrating the blend with a co-polymer solution and then allowing it to set.[18] Subsequently, the blend is analyzed by slicing with a band saw to reveal its internal structure.[19]

Experiments are performed using sieved fractions of glass beads that differ in color. The bulk density of each sample is determined by repeatedly filling and weighing a 1 liter container to provide a precise average. Similarly, the double-cone is completely filled with a single particle size and weighed to determine its capacity. In this manner, the quantities of each sample are determined by weight as a function of fill percentage.

The initial conditions are, as nearly as possible, identical in all experiments. The double-cone vessel is initially sprayed with an anti-static agent (Staticide, ACI, Elk Grove Village, II 60007) and the beads are loaded in two layers, large beads above small. To ensure reproducibility, the loading and storage of the beads is performed in an environmentally controlled chamber set to 70 °F and 60% relative humidity—these conditions were chosen to inhibit electrostatic charging of the particles. In each case, the blend consists of 70% by volume of the smaller beads, always loaded by weight. This fractional composition is chosen for two reasons, the first practical and the second theoretical. From the practical standpoint, higher percentages of large particles cause large particles to obscure underlying particles, making identification of patterns difficult. From the theoretical standpoint, in a 70/30 blend, it is possible to approximate the system as being a perturbed flow, dominated by the flow of the majority species. As we will see, this is useful for the development of a heuristic understanding of the mechanism leading to a peculiar segregation transition seen in the double-cone blender, described next.

III. RESULTS

In this section we describe the formation of steady segregation patterns in double-cones and the effects of both size ratio and absolute particle size on the formation of these patterns. For a given tumbler, blend composition, and fill fraction, the formation of steady asymptotic patterns are determined solely by the rotation speed of the blender. Three distinct pattern-forming regimes are specified: low, intermediate, and high speed. The transitions between these regimes are extremely sharp; a difference of half a revolution per minute is enough to cause a transition.

At low speeds, pattern formation is characterized by separation of components into an inner band of smaller particles surrounded by outer bands of larger particles, as shown for both blender sizes in Figs. 2(a)–2(b). We term this state

This article is copyrighted as indicated in the article. Reuse of AIP content is subject to the terms at: http://scitation.aip.org/termsconditions. Downloaded to IP: 132.203.227.63 On: Sun, 12 Jul 2015 01:44:53

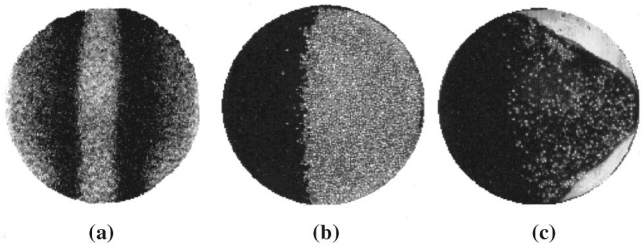

FIG. 3. Examples of other patterns observed. (a) Striped state in 4.3 l double-cone of 1.6 mm (light gray) and 0.6 mm (dark) beads at 24.0 rpm. (b) Asymmetric state in 4 mm (light gray) and 1.6 mm (dark) beads at 24.9 rpm. (c) Asymmetric state with upper strata of large beads removed, showing unbroken core of smaller grains.

''big-out.'' In this and in all other asymptotic states, the blend is radially segregated, with fines occupying the radial ''core,'' and the patterns are differentiated by axial segregated states.[20] This is shown in Figs. 2(c) and 2(f), where we display interior views after infiltrating the blend with solidifying polymer and slicing, as previously described. Although complete separation of the components is not produced, the outer regions are dominated by the large, light gray particles while the axial center is almost completely composed of smaller, dark particles.

At higher tumbling speeds, the blend spontaneously reverses its superficial segregation pattern, as shown in Figs. 2(d)–2(e). In this state, which we term ''small-out,'' radial segregation is again seen, with the fines occupying the radial center of the blender and the coarse grains the radial extremes.

The time needed for either pattern to become established is between 20 and 150 revolutions for tumbling speeds far from and near to the transition value, respectively.[21] The end of an experiment is visually determined by the formation of a steady surface segregation pattern that does not change over the course of 80 additional revolutions. In most cases, no stable intermediate pattern is ever observed: a slight change in tumbling speed causes grains to simply reverse axial positions in a discrete shift from ''big-out'' to ''small-out.''

The exact value of the transition speed depends on several factors, including the fill level, the tumbler size, the absolute size of the large particles, and the size ratio between particle species. In this paper, we focus on the dependence on particle size and size ratio, which appear to be the most revealing of the mechanisms at work.

Before we discuss the apparent mechanism in detail, we caution that segregation in fully 3D blenders can be remarkably complex, and our analysis is necessarily simplified. For example, if we vary the fill level or tumbler size along with the particle sizes, we find narrow parameter ranges in which more exotic states appear. The causes of these states are far from obvious; nevertheless they are easily reproduced using a simple model, presented in Sec. IV B. We display two of these in Fig. 3. In Fig. 3(a), we show a striped state that occurs in the large double-cone when rotated at 24.0 rpm and charged with 1.6 mm and 0.6 mm beads, while in Fig. 3(b) we show a left–right segregated state found for a blend of 4 mm and 1.6 mm beads rotated at 24.9 rpm.

The striped pattern can be sustained for long periods but appears to be metastable. This pattern is most commonly seen as an intermediate state that occurs during the formation of the small-out pattern. The left–right state, on the other hand, is very stable once established and seems to be generic in that it is also seen in tote blenders and V-blenders in our laboratory. This asymmetric state is found in both small-left and small-right alternatives and persists despite meticulous leveling of the apparatus (to within 0.2° of the horizontal). These novel states also exhibit strong radial segregation: in Fig. 3(c), for example, we have carefully removed nearly all the large beads, leaving an uninterrupted core of small dark grains that extends along the rotational axis of the blend. The ubiquitous presence of this core leads us to believe that, as in simple drum tumblers,[22] radial segregation develops first and is followed by the various axially segregated states that we report.

Analysis

With this caution in mind, we next turn to an analysis of the transition between the dominant (small-out and big-out) states, which are seen in the widest range of parameter space and whose mechanism seems to be the most comprehensible. To study this transition, we perform a number of experiments to evaluate a criterion for the onset of the the small-out state. These experiments were performed as follows: For each available diameter of small, ''bed'' particles, we choose a diameter of larger, ''intruder'' particles and layer this blend (large above small, as described previously) into the large double-cone. We produce a big-out pattern by tumbling the blend at a low speed for 100 revolutions and then increase the tumbling speed in subsequent experiments until we reach the ''onset'' speed of first occurrence of the small-out pattern. Finally, we refine this value to under 1 rpm in further repetitions of this procedure. The results of these experiments for numerous bed and intruder particle sizes are plotted in Fig. 4.

We observe two transitions in this figure. First, there is a cutoff size ratio below which no segregation pattern is seen at the surface.[23] In Figs. 4(b) and 4(c) we show snapshots of the surface of blends of 1.6 mm and 0.3 mm beads tumbled at 8 rpm and 40 rpm, respectively [at parameters indicated by asterisks in Fig. 4(a)]. The cutoff bed particle diameters are indicated by small arrows in Fig. 4: thus 6 mm intruders do not segregate in a bed of particles smaller than about 0.8 mm, and 1.1 mm intruders do not segregate in a bed of particles smaller than about 0.2 mm. We return to this observation in the final section of this paper.

Second, the onset speed of the small-out pattern varies considerably with bed and intruder particle sizes, but in all cases faster tumbling speeds lead to the small-out pattern and slower speeds lead to the big-out state. To make sense of these results, we anticipate that it may be possible to scale particle interactions with the ratio between particle diameters. This is by no means a foregone conclusion: for sufficiently small grains, for example, there is a competition be-

This article is copyrighted as indicated in the article. Reuse of AIP content is subject to the terms at: http://scitation.aip.org/termsconditions. Downloaded to IP: 132.203.227.63 On: Sun, 12 Jul 2015 01:44:53

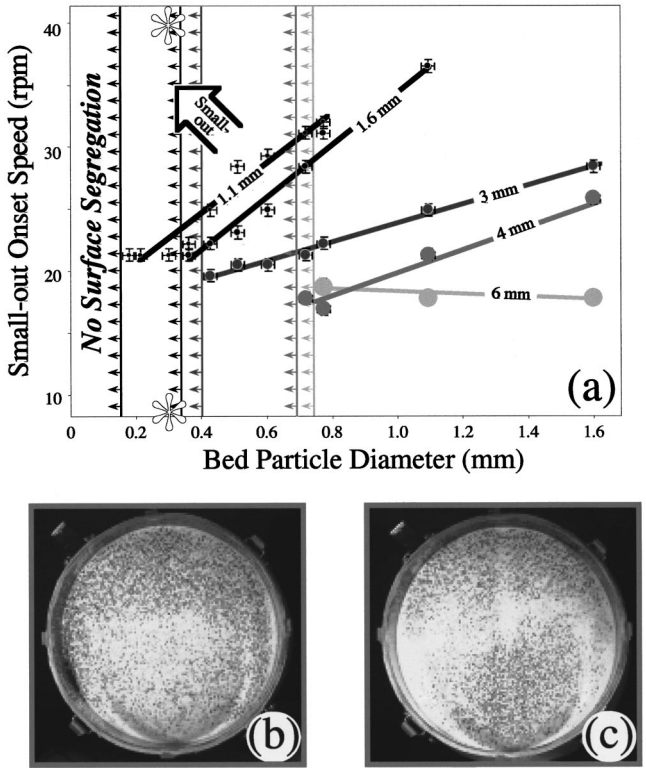

FIG. 4. (a) Onset tumbling speed of the small-out pattern in the large double-cone system as a function of bed particle diameter for several different intruder diameters. For each case, we indicate a cutoff bed particle diameter below which no significant surface segregation is seen. (b) The surface of a mixture of 1.6 mm (dark) and 0.3 mm (light gray) particles after 200 revolutions at (b) 8 rpm and (c) 40 rpm.

tween liquid bridging (which depends on contact area) and particle inertia (which depends on particle volume). Nevertheless, this simplest scaling hypothesis collapses most of the data of Fig. 4(a), as shown in Fig. 5. Evidently, for most of the bead sizes studied, the segregation process can be scaled in a simple way, suggesting both that the individual particle kinetics may be similar across scales and that the segregation may be scalable with tumbler size as well. To unveil the

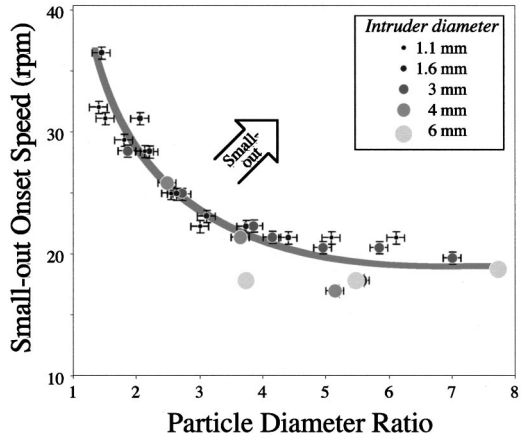

FIG. 5. Data from Fig. 4(a) rescaled as a function of the ratio of large-to-small particle diameters. The gray line is a spline to aid the eye.

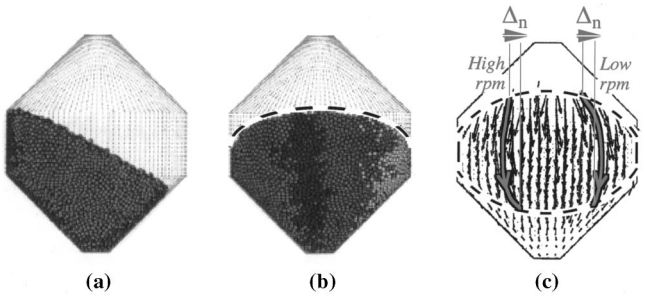

FIG. 6. (a) Side and (b) front view of double-cone in motion from particle dynamic simulations (presented elsewhere; see Ref. 24). Convex shape of free surface is indicated by dashed line in (b).

relevant particle kinetics, in the next section we inspect particle trajectories in detail.

IV. MECHANISMS OF SEGREGATION

A. Overview and heuristics

In Fig. 6 we display the results of particle-dynamic simulations[24] of flow of *mono*disperse spheres in the double-cone. Bidisperse simulations generate, for our purposes, similar results. In Figs. 6(a)–6(b) we see from side and front views, respectively, that the surface of the bed is nearly flat in the direction of convective flow [downhill, from left to right in Fig. 6(a)], but is typically convex in the transverse direction [indicated by the broken line in Fig. 6(b)]. The actual convexity seen in experiments is highly variable (and is most strongly affected by fill level), but the point to be stressed is that the flow of grains in the double-cone can be usefully divided into convective (azimuthal) and transverse (axial) components. Thus if we examine a typical time-averaged velocity field[25] near the surface of the granular bed, we obtain Fig. 6(c), which clearly shows an Eulerian velocity field in which particles travel in curved trajectories, roughly following the outlines of the container.

With this velocity field in mind, we can understand the observed segregation transition according to the following cartoon. At low tumbler speed, larger intruder grains roll atop the surface of the bed, following gravity. The bed surface for the half-filled tumblers that we consider tends to be convex [cf. Fig. 6(b)], so intruders roll toward the axial extremes of the blender as sketched in the gray arrow to the right of Fig. 6(c). Thus their net transport, Δ_n is *outward*, as indicated in the figure—simply because of bed geometry. At high tumbler speed, on the other hand, the larger grains will, all other things being equal, again move outward along the surface, but will travel faster downhill. Two things are observed to occur as a result. First, the large grains will reach the bottom of the granular cascade with less outward displacement than in slower tumblers, and second these intruders will rebound significantly when they reach the curved surface of the blender. Thus as sketched in gray to the left of Fig. 6(c), intruders travel down the cascade along a less curved trajectory than at lower tumbler speeds, and are diverted inward once they reach the end of their travel. This produces a net *inward* transport, Δ_n, as indicated by an arrow in the figure.

This article is copyrighted as indicated in the article. Reuse of AIP content is subject to the terms at: http://scitation.aip.org/termsconditions. Downloaded to IP: 132.203.227.63 On: Sun, 12 Jul 2015 01:44:53

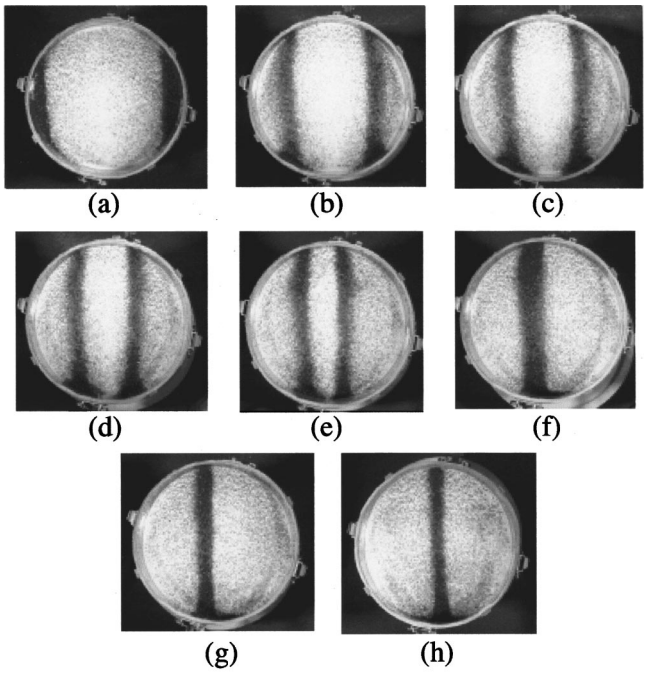

FIG. 7. Successive snapshots of inward migration of dark, 1.6 mm, intruders in bed of light gray, 3.7 mm, glass beads as blender speed is increased. (a) The blender is initially prepared by tumbling the blend at 8 rpm for 80 revolutions, after which it is tumbled at 21.3 rpm for (b) 40, (c) 80, (d) 120, (e) 160, (f) 200, and (g) 280 revolutions. In (h) the blender is further run at 25.8 rpm for 80 revolutions.

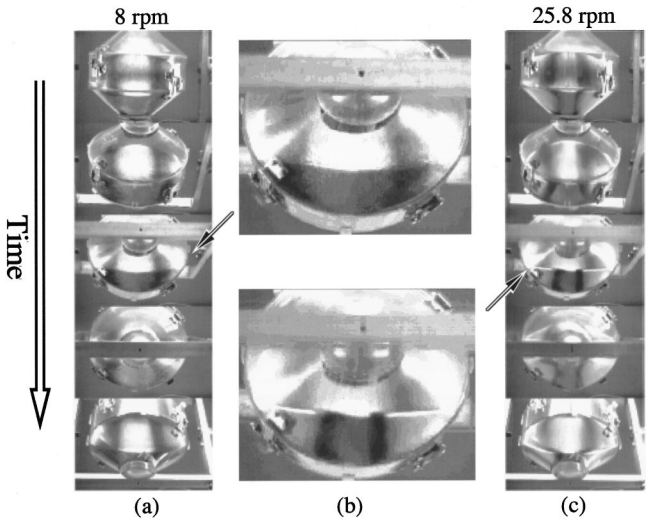

FIG. 8. Two time series of double-cone (rotated from top to bottom in these views) taken during flow of a blend of 1.6 mm (dark) and 0.4 mm (light gray) glass beads at 8 and 25.8 rpm, as indicated. (a) At 8 rpm, larger particles re-entering the bed flare *outward*, away from the tumbler centerline, while (c) at 25.8 rpm, larger particles converge *inward* (arrows). Sequential frames correspond approximately to 0, 0.11, 0.20, 0.26, and 0.38 revolutions, and enlarged views of the 0.20 revolution case are shown in (b) for the two different speeds.

We investigate the accuracy of this cartoon in the following experiments. First, in Fig. 7, we show a time sequence from an experiment in which a blend of 1.6 mm diameter glass intruders (dark) in a bed of 0.37 mm glass beads (light gray) is initially prepared in the big-out pattern by rotating at 8 rpm. In this time sequence, the bed is tumbled at 21.3 rpm for increasing durations. Evidently at the higher tumbling speed, large (dark) grains travel in nearly straight paths down the cascade, and undergo a net transport inward.

Moreover, in Fig. 8 we display digital video sequences at low (8 rpm) and high (25.8 rpm) speeds. These sequences show that at low tumbler speeds [Fig. 8(a)] the dark intruders move *outward*, while at high speeds [Fig. 8(c)] the same intruders move sharply *inward* after collision with the downstream boundary. This is visible at all phases of rotation, but is most strongly seen at the points identified by the arrows in the figure and enlarged in Fig. 8(b).

The increase in net outward transport of intruders as the tumbler speed is diminished is also made visible in Fig. 9, where we display the converse of the behavior shown in Fig. 8. Here, we prepare a blend of 1.6 mm intruders (light gray) and 0.6 mm beads (dark) bed particles in the small-out state by tumbling the large double-cone at 28.4 rpm for 100 revolutions [Figs. 9(a)–9(b)]. We then show snapshots of the segregation pattern after 1/2 revolution at several, diminishing, tumbling speeds [Figs. 9(c)–9(f)]. Evidently as the tumbling speed is reduced, and the light gray intruders leave the cascade and become entrained in the static portion of the granular blend, they increasingly flare outward to form a bulge, identified by arrows in the figure.

Thus at low speeds, intruders prepared in the small-out state spread sharply outward [Figs. 8(a), 9], while at high speeds, intruders prepared in the big-out state converge inward [Figs. 7, 8(c)]. From this phenomenology together with our cartoon of Fig. 6(c), it is straightforward to construct and investigate a computational model for the mechanism. We describe such a simplified model next.

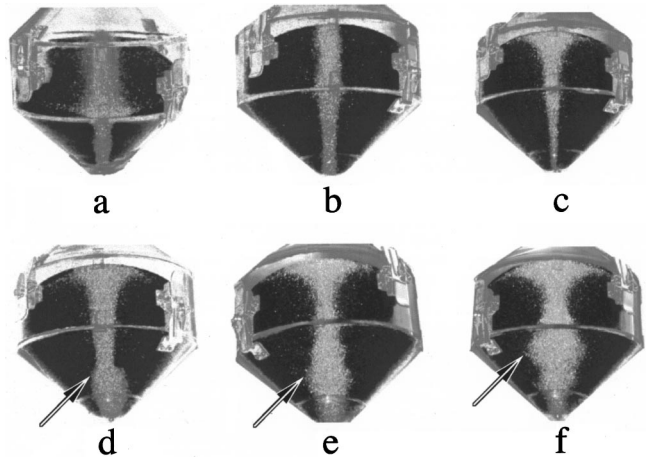

FIG. 9. Surface segregation pattern for a mixture of 1.6 mm (light gray) and 0.6 mm (dark) glass spheres from (a) front and (b) back of tumbler after tumbling for 100 revolutions at 28.4 rpm. Changes seen in the segregation pattern (back view) when run for 1/2 revolution [starting repeatedly from the state shown in (a) and (b)] at (c) 28 rpm, (d) 16 rpm, (e) 12 rpm, and (f) 8 rpm. Arrows identify bulge referred to in text.

This article is copyrighted as indicated in the article. Reuse of AIP content is subject to the terms at: http://scitation.aip.org/termsconditions. Downloaded to IP: 132.203.227.63 On: Sun, 12 Jul 2015 01:44:53

B. Lowest order model

To construct the model, we initially distribute a number of ''intruder'' particles in a unit circular domain.[26] This domain is a simplified representation of the surface of the double-cone, on which nearly all flow—and therefore nearly all segregation—is believed to occur.[27] We stress that in this model we explicitly track only the large intruder particles and assume that the bed merely acts as a substrate on which the intruders roll. Some implicit deformation of the bed is considered as an embellishment on the model (see below), but this is not necessary to generate the big-out/small-out transition, which we find is very robust.

Flow on the unit circle domain obeys the following three explicit rules.

Rule 1: The dominant convective flow is assumed to occur at fixed speed, $-V_y$, in the *vertical* direction, and the domain is taken to be periodic in this direction, so that particles that exit the bottom of the circle at the location $(X, -Y)$ re-emerge at its top at (X,Y). Thus for each particle, i, at discrete time, n, the vertical coordinate is modified according to

$$Y_i(n+1)=Y_i(n)-V_y + \begin{cases} 2\sqrt{1-X_i(n)^2} & \text{if } (X_i(n)^2+Y_i(n)^2>1) \\ 0 \quad \text{otherwise} \end{cases} + \eta_{yi}(n), \tag{1}$$

where $\eta_{yi}(n)$ is a random term included to account for collisional diffusion and taken uniformly from $[-\eta_{\max},\eta_{\max}]$, where $\eta_{\max}$ is a constant whose value is given below.

Rule 2: *Horizontal* flow occurs in one of two ways: (a) the assumed convexity of the free surface draws particles horizontally outward at a prescribed rate, toward the axial extremes of the surface; and (b) when particles reach the bottom wall of the circular domain, they rebound inelastically and specularly. Both of these effects are defined by the following expression:

$$X_i(n+1)=X_i(n)+C_i(n)+R_i(n)+\eta_{xi}(n), \tag{2}$$

where $C_i(n)$ defines the effects of bed convexity (described below), $R_i(n)$ defines the specular reflection of particles from the domain boundary, and, as for the vertical case, $\eta_{xi}(n)$ is a random term uniformly taken from $[-\eta_{\max},\eta_{\max}]$.

Rule 3: As intruder particles migrate across the tumbler surface, they are assumed to displace bed particles, the conservation of which implies that the bed should enlarge (shrink) in response in regions sparsely (densely) populated by intruders. To accommodate this effect, we define the convexity function to be

$$C_i(n)=C\cdot\text{sign}(X_i(n))\cdot\{-X_i(n)^2+[X_i(n)\cdot(1+\epsilon)]^4 - A\cdot[1-\rho_i(X)]\}, \tag{3}$$

where the density, $\rho_i(X)$, is a cubic spline to a coarse grained average over large neighborhoods of intruders. Explicitly, we divide the width of the unit circle into m bins, measure the normalized density, R_j, of intruders within each bin, and define $\rho_i(X)$ to be a cubic spline to the set of points $\{(-1,0),(-1+1/m,R_1),(-1+3/m,R_2),\ldots,(1,0)\}$. We have investigated several choices of the number of bins, m, across the width of the unit circle. In what follows, we present the simplest possible scenario,[28] in which $m=2$. For larger values of m, the patterns we show are augmented by more finely scaled stripes. Since in this paper we seek only the lowest order segregation states, we have chosen to examine only the lowest order choices for our model.

Finally, we define the reflection term to be

$$R_i(n)=V_y\cdot\beta\cdot\text{sign}[X_i(n)]\cdot\cos[2\cdot|\sin^{-1}(X_i(n))|-\pi/4], \tag{4}$$

where β is a coefficient of restitution.

For parameter choices in our simulations, we use the representative values[29] $\beta=0.5$, $C=0.01$, and $A=0.1$. The constant ϵ is included for a technical reason: if intruders are allowed to approach sufficiently close to $X=\pm1$, the algorithm that generates periodicity [braces in Eq. (1)] breaks down, and intruders can escape from the unit circle. We fix $\epsilon=0.05$, which effectively prevents this anomaly.

In Fig. 10 we display results of this model for several choices of V_y using 621 intruder particles initially distributed in the unit circle as described previously. Beneath each snapshot we show a plot of the instantaneous density (evaluated in ten bins across the width of the unit circle and fit with a cubic spline). From left to right in Fig. 10, we see the big-out segregation pattern, followed by a big-right state, a three-stripe pattern, a big-left state, and a small-out pattern. The big-out state seen at the lowest convective speeds is produced when the convexity term $C_i(n)$ exceeds the reflection term, $R_i(n)$, causing particles to fall into the two potential wells of the quartic convexity function in Eq. (3). As the convective speed increases, a metastable three-stripe pattern appears, which gives way to the symmetry-breaking state seen on $0.07\leqslant V_y\leqslant 0.09$. With the exception of the transient state [Fig. 10(c)] all of the other snapshots are taken after the same equivalent distance of travel of intruder particles, i.e., at constant n/V_y and with all other parameters held fixed. The noise parameter is chosen to be $\eta_{\max}=0.025$ for all cases except the transient state; this state is less distinct than the others, so for Fig. 10(c) we let $\eta_{\max}=0.01$, which accentuates the three-stripe pattern (cf. Fig. 12 below also).

C. Bifurcation analysis

From our model, we interpret these patterns to be produced by a competition between convexity of the bed surface—tending to drive particles away from the tumbler center—and collisions with the circular boundary of the flow domain—tending to draw particles toward the tumbler center. Since the model is comparatively simple, it is possible to draw analytic conclusions. In one cycle across the unit circle, an intruder travels outward a distance:

$$\Delta X=R_i(n)+\sum_{n}^{D/V_y} C_i(n), \tag{5}$$

This article is copyrighted as indicated in the article. Reuse of AIP content is subject to the terms at: http://scitation.aip.org/termsconditions. Downloaded to IP: 132.203.227.63 On: Sun, 12 Jul 2015 01:44:53

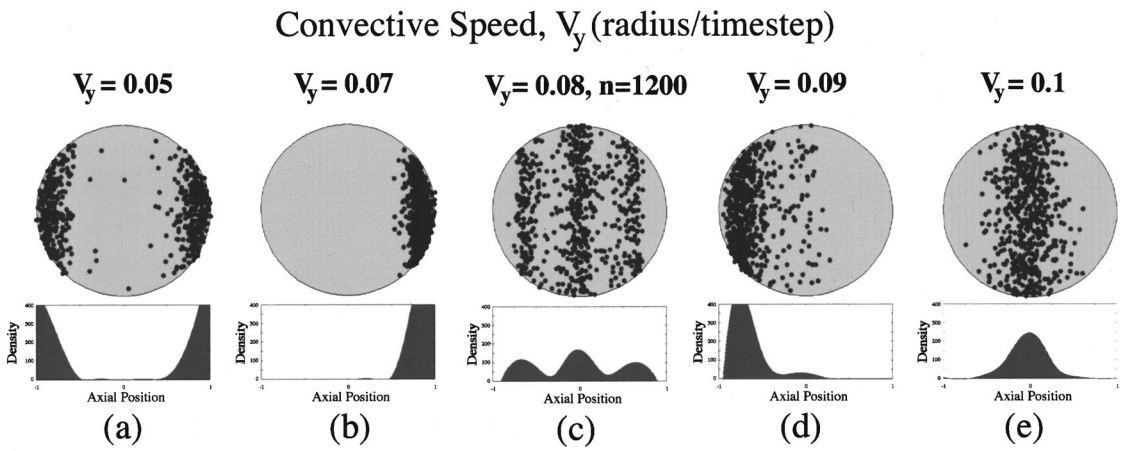

FIG. 10. Results of simplified model simulation described in text. Patterns seen include (a) the big-out, (b) the big-right, (c) the three-stripe, (d) the big-left, and (e) the small-out states. All plots except (c) are taken after the same equivalent distance of travel of intruder particles. Plot (c) is shown after $n=1200$ time steps: about 10% of the periods are shown in the other plots.

where D is the vertical distance traveled by the intruder from entry to exit from the unit circle. Neglecting the density and diffusion terms, all of the quantities in Eqs. (3)–(5) depend only on $X_i(n)$ and the known constants. At low V_y, $C_i(n)$ reduces to an expression similar to the Landau–Ginzburg form, which naturally leads to the big-out pattern with intruders centered around $X\approx\pm 0.9$. As V_y increases, the transitions differ in detail from a Landau–Ginzburg phase transition, but in substance the two transitions are similar.

The qualitative form of the expected bifurcations is shown in Fig. 11(a), where we plot ΔX from Eq. (5) for several values of V_y using the approximation $D=(1+\sqrt{1-X^2})$. At $V_y\approx 0.01$, the slope $d(\Delta X)/dx$ changes sign and the fixed point, P_i, at the origin first becomes locally stable as new, unstable, fixed points P^* are born in a subcritical pitchfork bifurcation. At $V_y\approx 0.09$, the stable and unstable fixed points, P_s and P_u, respectively, annihilate in a (reverse) saddle-node bifurcation. Thus in the range $0.01<V_y<0.09$, *both* the inner fixed point P_i *and* the outer ones P_s coexist and are locally stable. Above $V_y\approx 0.09$, P_i is the sole remaining fixed point and is globally stable.

This analysis is only approximate (e.g., D is known in closed form and ρ is lowest order), but heuristically describes the behaviors seen in experiments and is in agreement with our observations. For example, in Fig. 12 we plot model segregation plots for several cases with the density or diffusion terms removed. As anticipated from the preceding discussion, at $V_y=0.01$, only a tiny remnant of a central fixed point is seen [Figs. 12(a), 12(b)], which is completely destabilized by added noise up to considerably larger values of V_y [cf. Fig. 10(a)]. As V_y increases, the coexistence of fixed points P_i and P_s becomes evident and the outer fixed points P_s moves axially inward until $V_y\approx 0.09$, at which point the outer points P_s disappear and only the central fixed point remains.

In the presence of additive noise [$\eta_{xi}(n)$ in Eq. (2)], the analysis changes only quantitatively: The locations and stability of the fixed points are unchanged, but the narrow basin of P_i allows particles to escape[30] to the fixed point, P_o, with larger basin of attraction and greater stability (for example at

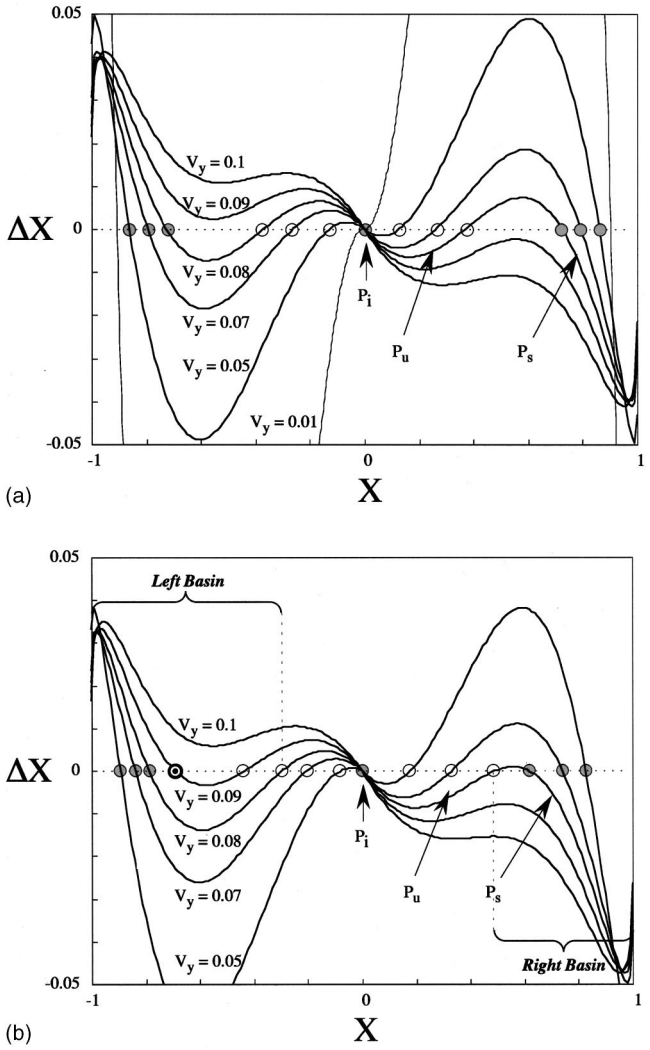

FIG. 11. Approximate phase plot generated by model flow. ΔX is the net horizontal distance displaced by an intruder in one pass through the granular bed. (a) Phase plot for symmetric convexity term; (b) phase plot for asymmetric convexity, as might be produced by displacement of bed particles by intruders. Left and right basins of attraction are shown for the case $V_y=0.08$, and the remaining stable fixed point on the left is highlighted (bull's eye) at $V_y=0.09$. Plots (b)–(e) are taken after the same equivalent distance of travel of intruder particles. Plot (a) is shown after $n=1000$ time steps: about 4% of the periods are shown in the other plots.

This article is copyrighted as indicated in the article. Reuse of AIP content is subject to the terms at: http://scitation.aip.org/termsconditions. Downloaded to IP: 132.203.227.63 On: Sun, 12 Jul 2015 01:44:53

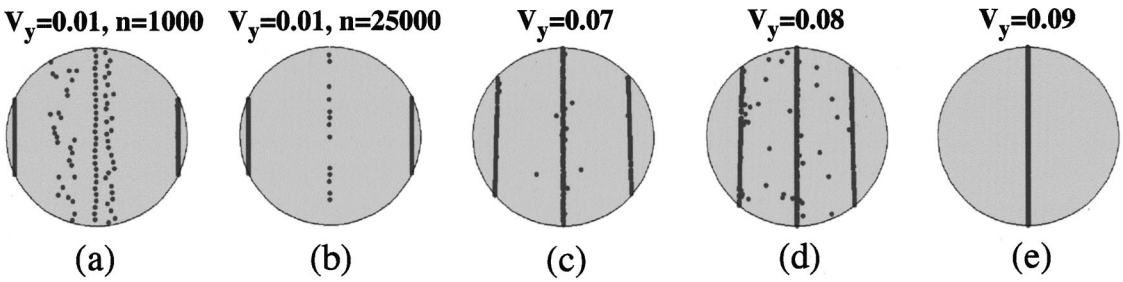

FIG. 12. Snapshots of model surface segregation patterns without density or diffusion terms. Scatter in intruder positions is due to slight added variation in *initial* particle placements, as mentioned earlier in text.

$V_y = 0.05$, the Lyapunov number for P_s is over 0.4, while for P_i it is 0.04).

If changes in convexity due to displacement of bed particles [$\rho_i(X)$ in Eq. (4)] are included, on the other hand, qualitatively new states arise. In Fig. 11(b) we plot phase portraits for the ansatz: $\rho = 0.05 \cdot X$. Naturally, more complicated densities are possible; in the spirit mentioned previously we seek the simplest possible states and consequently we use the simplest nontrivial expression for ρ. In this case, the phase portraits change little for large V_y: the small-out state prevails. For moderate or small V_y, on the other hand, strong asymmetry is enforced, causing the basins of attraction to the fixed points, P_s, in the positive half-plane to be compressed close to $X = +1$, while the basins of attraction in the negative half-plane broaden. This contrast becomes increasingly pronounced until $V_y \approx 0.09$, at which point the right basin of attraction vanishes in a reverse saddle-node bifurcation, leaving the left basin intact. For this choice of V_y, there are two fixed points at or left of the origin and none right of it. This corresponds to the left–right state of Figs. 3(b) and 10(d).

D. Segregation cutoff

Experimental and modeling results indicate that the choice of segregation pattern in the double-cone depends on the magnitude of the convective, azimuthal, velocity, V_y. In addition, we have seen [Fig. 4(a)] that there is a cutoff size ratio beyond which visible segregation patterns vanish. This cutoff remains unexplained. To better understand this effect, we carried out separate experiments in *cylindrical* tumblers to determine the precise value and dependence of surface flow on particle size ratio in the simplest possible context. Results of this exercise are summarized in Figs. 13 and 14. In Fig. 13, we hold the mean bed particle diameter fixed and vary the diameter of a small number of sparsely distributed intruders, while in Fig. 14 we hold the intruder size fixed and vary the diameter of bed particles. In Fig. 13 we plot the surface speed of isolated glass intruders as a function of distance along the streamwise direction in a 95 mm drum half filled with 920 μm glass beads at two different tumbling speeds.

Three things are evident here. First, intruders naturally travel more rapidly downstream at higher tumbler speed. Second, the distance, d_{rpm}, over which intruders are found at the surface is inversely related to tumbler speed. This dependence is shown in the inset to Fig. 13 for the case of 4 mm intruders. It is not known whether this inverse relationship is due to reduced shear in the flowing layer at higher speed, to reduced time for radial segregation to operate, or to another, as yet undetermined, effect.

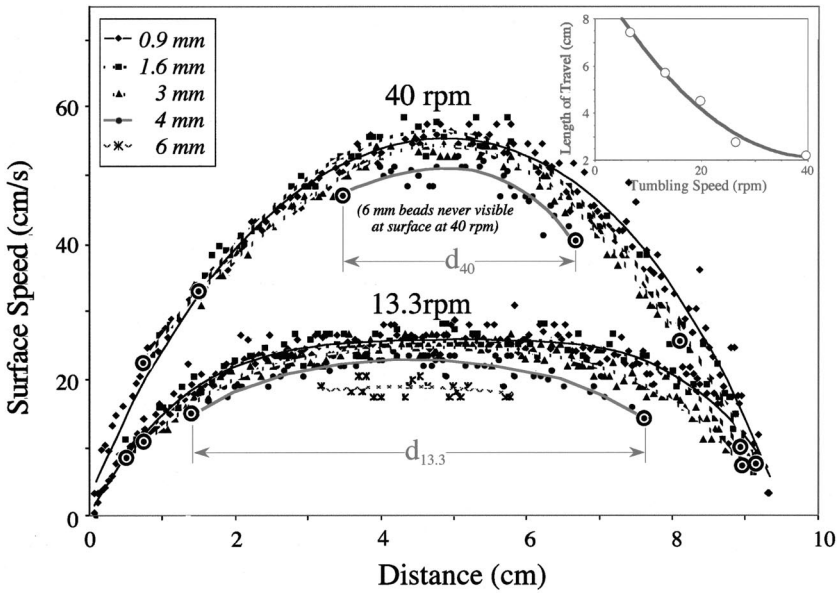

FIG. 13. Surface speeds of isolated (low concentration) glass beads of sizes indicated in legend in long, 95 mm diameter drum half filled with 920 μm glass beads. At low rotation rates, *s*, particles reach their terminal speed rapidly and remain at that speed during much of the cascade, while at higher rotation rates particles continually accelerate. At both extremes in rotation rate, particle speeds vary only modestly with particle size, however, the *distances*, d_s, over which the particles travel near the surface change dramatically with rotation rate, as indicated in the plot for the example of 4 mm beads. Curves are fourth order polynomial fits. Inset shows lengths of travel (denoted d_n in main plot) vs tumbling speed for 4 mm intruders; the fit here is with a cubic spline.

This article is copyrighted as indicated in the article. Reuse of AIP content is subject to the terms at: http://scitation.aip.org/termsconditions. Downloaded to IP: 132.203.227.63 On: Sun, 12 Jul 2015 01:44:53

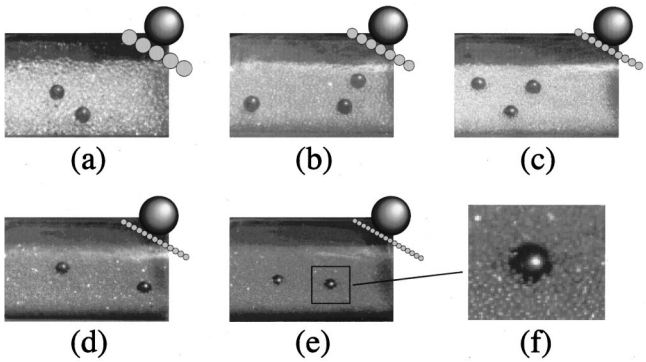

FIG. 14. Surface positions of dark 4 mm glass spheres tumbled in 25 mm diameter, 55 mm long glass vials 50% filled with beds of (a) 1.6 mm, (b) 1.1 mm, (c) 0.8 mm, (d) 0.6 mm, and (e) 0.5 mm glass spheres. (f) Expanded view of partially buried intruder from (e). Insets depict relative sizes of intruder and bed particles.

Third, and most significantly, larger intruders travel *more slowly* with respect to the free surface than smaller intruders. This may be due to the fact that larger intruders sample over a greater depth through the bed (and cascading speeds are known to diminish with depth into the bed[31]). The limiting case of very large intruders produces blends in which the intruders never emerge at the surface of the bed at all. In Fig. 13, this is seen at 40 rpm for the case of 6 mm intruders. Since we have argued that segregation occurs due to different velocity histories of bed and intruder particles in the cascade, the observation that segregation is shut down at large size ratios follows as a natural outcome of the failure of intruders to emerge at the bed surface, where they can flow comparatively freely.

The root cause of this segregation cutoff is not completely clear, however, and to further investigate the effect we have performed a final set of experiments in which we magnify the cascade in sparse blends of fixed size intruders in beds of increasingly finer beads. Results of this exercise are summarized in Fig. 14. Evidently, at low ratio R_{ib}=intruder-diameter/bed-diameter, intruders roll freely on top of the cascading bed layer. For example, in Fig. 14(a), $R_{ib}=2.5$, and the bed particles form a comparatively smooth substructure on which the intruders can travel. As R_{ib} grows, however, the bed particles approach a continuum (see insets) on the scale of the intruder, and the intruders *sink into* this substrate, as seen in enlargement, Fig. 14(f). This tendency of large particles to sink into fine beds seems significant and will be a topic of future study.

V. OUTLOOK

In this article, we used a combination of experiments, simplified models, and simulations to describe the processes that lead to segregation of particles of unequal size in a commercially relevant blender geometry. As demonstrated by the variety of results presented here, spontaneously occurring segregation patterns can be remarkably complex, with transitions that depend sensitively on fine modifications of process parameters. Despite the complexity in outward states, the process of segregation can evidently be understood by systematic analysis of the key differential kinetics of the particle species in the blend. In the double-cone blender, the kinetics at work seems to consist of a competition between an outward cascade down the convex free surface with an inward rebound against the concave downstream boundary of the blender. In other geometries and flows, the kinetics will of course differ. Nevertheless, through this case study we have seen that, by dissecting the flow and identifying mechanisms by which different species of particles follow different trajectories, it is possible to construct reasonably simple and workable models for the understanding of complicated granular phenomena.

ACKNOWLEDGMENTS

We acknowledge E. Spartalis, M. Geftic, J. O'Leary, and M. Moakher for technical assistance, and Pfizer, Inc. and the International Fine Particle Research Institute for financial support. We also thank D. Brone, who first identified several of the segregation states discussed here.

[1] H. Moritomi, T. Iwase, and T. Chiba, ''A comprehensive interpretation of solid layer inversion in liquid fluidized beds,'' Chem. Eng. Sci. **37**, 1751 (1982); R. H. Jean and L-S. Fan, ''A simple correlation for solids holdup in a gas-liquid-solid fluidized bed,'' *ibid.* **41**, 2823 (1986).

[2] M. Moakher, T. Shinbrot, and F. J. Muzzio, ''Experimentally validated computations of flow, mixing and segregation of non-cohesive grains in 3D tumbling blenders,'' Powder Technol. **109**, 58 (2000); J. C. Williams, ''The segregation of particulate materials. A review,'' *ibid.* **15**, 245 (1976); J. Bridgwater, ''Fundamental powder mixing mechanisms,'' *ibid.* **15**, 215 (1976).

[3] S. B. Savage and C. K. K. Lun, ''Particle size segregation in inclined chute flow of dry cohesionless granular solids,'' J. Fluid Mech. **189**, 311 (1988).

[4] A. W. Alexander, M. Roddy, D. Brone, J. Michaels, and F. J. Muzzio, ''A method to quantitatively describe powder segregation during discharge from vessels,'' Pharmaceutical Technology, Supplement, October 2000, pp. 6–21; P. Arteaga and U. Tuzun, ''Flow of binary mixtures of equal-density granules in hoppers—Size segregation, flowing density, and discharge rates,'' Chem. Eng. Sci. **45**, 205 (1990); K. Shinohara, K. Shoji, and T. Tanaka, ''Mechanism of segregation and blending of particles flowing out of mass-flow hoppers,'' Ind. Eng. Chem. Process Des. Dev. **9**, 174 (1970); ''Mechanism of size segregation of particles in filling a hopper,'' *ibid.* **11**, 369 (1972); J. F. G. Harris and A. M. Hildon, ''Reducing segregation in binary powder mixtures with particular reference to oxygenated washing powders,'' *ibid.* **9**, 363 (1970); J. M. Rotter, J. M. F. G. Holst, J. Y. Ooi, and A. M. Sanad, ''Silo pressure predictions using discrete-element and finite-element analyses,'' Philos. Trans. R. Soc. London, Ser. A **356**, 2685 (1998).

[5] J. Bridgwater, N. W. Sharpe, and D. C. Stocker, ''Particle mixing by percolation,'' Trans. Inst. Chem. Eng. **47**, T114 (1969); J. Knight, H. Jaeger, and S. Nagel, ''Vibration-induced size separation in granular media: The convection connection,'' Phys. Rev. Lett. **70**, 3728 (1993); R. Jullien and P. Meakin, ''Three-dimensional model for particle-size segregation by shaking,'' *ibid.* **69**, 640 (1992); D. Brone and F. J. Muzzio, ''Size segregation in vibrated granular systems: A reversible process,'' Phys. Rev. E **56**, 1059 (1997); T. Shinbrot and F. J. Muzzio, ''Reverse buoyancy in shaken granular beds,'' Phys. Rev. Lett. **81**, 4365 (1998).

[6] A. W. Chester, J. A. Kowalski, M. E. Coles, E. L. Muegge, F. J. Muzzio, and D. Brone, ''Mixing dynamics in catalyst impregnation in twin-cone blenders,'' Powder Technol. **102**, 85 (1999); D. Brone and F. J. Muzzio, ''Enhanced mixing in double cone blenders,'' *ibid.* (in press); K. W. Carley-Macauly and M. B. Donald, ''The mixing of solids in tumbling mixers—I,'' Chem. Eng. Sci. **17**, 493 (1962); K. J. Sethuraman and G. S. Davies, ''Studies on solids mixing in a double-cone blender,'' Powder Technol. **5**, 115 (1971).

[7] M. D. Ashton and F. H. H. Valentin, ''The mixing of powders and particles in industrial mixers,'' Trans. Inst. Chem. Eng. **44**, T166 (1966); J. B. Gray, ''Performance of dry solids mixing equipment,'' Chem. Eng. Prog.

This article is copyrighted as indicated in the article. Reuse of AIP content is subject to the terms at: http://scitation.aip.org/termsconditions. Downloaded to IP: 132.203.227.63 On: Sun, 12 Jul 2015 01:44:53

53, 25 (1957); A. Kaufman, ''Mixing of solids,'' Ind. Eng. Chem. Fundam. **1**, 104 (1962).
[8]T. Ramanujam, S. Davies, and D. Venkateswarlu, Indian J. Technol. **7**, 218 (1969).
[9]M. Moakher, T. Shinbrot, and F. J. Muzzio, ''Experimentally validated computations of flow, mixing and segregation of noncohesive grains in 3D tumbling blenders,'' Powder Technol. **109**, 58 (2000).
[10]M. B. Donald and B. Roseman, ''Mixing and de-mixing of solid particles,'' Br. Chem. Eng. **7**, 749 (1962); S. D. Gupta, D. V. Khakhar, and S. K. Bhatia, ''Axial segregation of particles in a horizontal rotating cylinder,'' Chem. Eng. Sci. **46**, 1513 (1991); N. Nakagawa, ''Axial segregation in a horizontal rotating cylinder,'' *ibid.* **49**, 2540 (1994).
[11]K. M. Hill and J. Kakalios, ''Reversible axial segregation of rotating granular media,'' Phys. Rev. E **52**, 4393 (1995).
[12]J. H. Bytnar, J. O. G. Parent, H. Henein, and J. Iyengar ''Macrosegregation diagram for dry blending particulate metal-matrix composites,'' Int. J. Powder Metall. **31**, 37 (1995).
[13]Defined for this problem to be $\mathrm{Fr}=\omega^2 r/2g$, where ω is the drum angular velocity, r is its radius, and g is gravitational acceleration.
[14]J. T. Carstensen and M. R. Patel, ''Blending of irregularly shaped particles,'' Powder Technol. **17**, 273 (1977).
[15]J. C. Williams and M. I. Khan, ''The mixing and segregation of particulate solids of different particle size,'' Chem. Eng., London **269**, 19 (1973).
[16]D. Brone and F. J. Muzzio, ''Enhanced mixing in double cone blenders,'' Powder Technol. **110**, 79 (2000).
[17]Below 8 rpm, motion is intermittent, and above 40 rpm, the surface flow is not steady.
[18]C. Wightman, F. J. Muzzio, and J. Wilder, ''A quantitative image analysis method for characterizing mixtures of granular materials,'' Powder Technol. **89**, 165 (1996).
[19]This freezing and slicing method is not feasible on the larger vessels because sacrificing the blender is prohibitively expensive and because large polymeric masses tend to set nonuniformly.
[20]Observed previously in M. Moakher, T. Shinbrot, and F. J. Muzzio, ''Experimentally validated computations of flow, mixing and segregation of non-cohesive grains in 3D tumbling blenders,'' Powder Technol. **109**, 58 (2000).
[21]cf., e.g., S. H. Strogatz, *Nonlinear Dynamics and Chaos* (Addison-Wesley, Reading, MA, 1994), pp. 99 ff.
[22]K. M. Hill, A. Caprihan, and J. Kakalios, ''Bulk segregation in rotated granular material measured by magnetic resonance imaging,'' Phys. Rev. Lett. **78**, 50 (1997); A. W. Chester, J. A. Kowalski, M. E. Coles, E. I. Muegge, F. J. Muzzio, and D. Brone, ''Mixing dynamics in catalyst impregnation in twin-cone blenders,'' Powder Technol. **102**, 85 (1999); S. D. Gupta, D. V. Khakhar, and S. K. Bhatia, ''Axial segregation of particles in a horizontal rotating cylinder,'' Chem. Eng. Sci. **46**, 1513 (1991).
[23]C. M. Dury and G. H. Ristow, ''Competition of mixing and segregation in rotating cylinders,'' Phys. Fluids **11**, 1387 (1999); K. M. Hill, A. Caprihan, and J. Kakalios, ''Bulk segregation in rotated granular material measured by magnetic resonance imaging,'' Phys. Rev. Lett. **78**, 50 (1997).
[24]M. Moakher, T. Shinbrot, and F. J. Muzzio, ''Experimentally validated computations of flow, mixing and segregation of noncohesive grains in 3D tumbling blenders,'' Powder Technol. **109**, 58 (2000).
[25]Details in Ref. 24.
[26]Specifically, we place particles on a square Cartesian grid and then adjust the X and Y coordinate of each particle by an amount δ chosen at random on $[-0.02,0.02]$.
[27]M. Nakagawa, S. A. Altobelli, A. Caprihan, E. Fukushima, and E-K. Jeong, ''Non-invasive measurements of granular flows by magnetic resonance imaging,'' Exp. Fluids **16**, 54 (1993); M. Moakher, T. Shinbrot, and F. J. Muzzio, ''Experimentally validated computations of flow, mixing and segregation of noncohesive grains in 3D tumbling blenders,'' Powder Technol. **109**, 58 (2000); T. Shinbrot, A. Alexander, and F. J. Muzzio, ''Spontaneous chaotic granular mixing,'' Nature (London) **397**, 675 (1999).
[28]cf. J. Eggers, ''Sand as Maxwell's demon,'' Phys. Rev. Lett. **83**, 5322 (1999).
[29]Effects of changes in these values will be discussed elsewhere.
[30]K. Wiesenfeld and F. Moss, ''Stochastic resonance and the benefits of noise: From ice ages to crayfish and SQUIDs,'' Nature (London) **373**, 33 (1995); F. J. Romeiras, C. Grebogi, E. Ott, and W. P. Dayawansa, ''Controlling chaotic dynamical systems,'' Physica D **58**, 165 (1992).
[31]M. Nakagawa, S. A. Altobelli, A. Caprihan, E. Fukushima, and E-K. Jeong, ''Noninvasive measurements of granular flows by magnetic resonance imaging,'' Exp. Fluids **16**, 54 (1993).

This article is copyrighted as indicated in the article. Reuse of AIP content is subject to the terms at: http://scitation.aip.org/termsconditions. Downloaded to IP: 132.203.227.63 On: Sun, 12 Jul 2015 01:44:53